Tackling the Challenges of Deployable Thin-Film Space Structures with Abaqus

Dr. Chiachung Lee*, Mike Sasdelli†

* - Stinger Ghaffarian Technologies, Inc.

† - Dassault Systèmes Government Solutions, Inc.

***Abstract**: In order to support challenging requirements for space science missions, NASA and its industry partners are turning to deployable thin-film structures. A good example is the sunshield for the James Webb Space Telescope (JWST). The sunshield provides the necessary screening from external light and heat sources required to ensure proper functioning of the telescope. It is comprised of multiple layers of very thin (0.001-0.002 inch) Kapton film and has a deployed plan-form area roughly equivalent to a tennis court. In order to fit within the launch vehicle payload envelope of course this large-area structure must be stowed in a folded configuration then deployed to full plan-form once on orbit.*

The uniqueness of the structure both in terms of function, extreme "flimsiness" and the necessity of performing in the zero-G space environment make design and testing very challenging. The value of simulation software like Abaqus is tremendous in such an engineering scenario both in terms of reducing the time and expense of testing, allowing simulation of difficult or impossible test environments (e.g., zero-G) and expediting insights facilitating design improvement. This paper will explore the extreme challenges of simulating the behavior of the sunshield structure, and structures like it, and demonstrate the powerful solution capabilities of Abaqus, in particular its evolving general contact algorithms, in the context of those challenges.

***Keywords**: Spacecraft, Thin films, Contact analysis*

1. Introduction

The James Webb Space Telescope (JWST) is a collaborative effort of NASA, the European Space Agency (ESA) and the Canadian Space Agency (CSA), planned for launch in October 2018. JWST will allow astronomers to study the history of the universe from the early stages of the Big Bang to the emergence of our solar system. Figure 1 provides an illustration of the spacecraft and its primary sub-systems.

One of the key sub-systems of the spacecraft is the sunshield. Composed of 5 layers of a specially coated, very thin Kapton film covering an area equivalent to a tennis court, the sunshield essentially provides a thermal barrier between the sun-side of the spacecraft (typically around 358 K or 185 ºF) and the cold side where the optical and science instruments reside in an thermally stable operating environment that must be kept below 50 K (-370 ºF) to ensure proper functioning.

The successful engineering of the JWST required understanding the folding and deployment characteristics of the sunshield film. While much can be learned from laboratory testing of the films, testing has its limits for such structures including cost and testing deployment in the 0-g environment of space. As such, successful methods of simulating the film behavior via tools like finite element analysis can contribute invaluable insights to engineering decision-making. In this paper, we will discuss the challenges of performing finite element analyses for this particular structure and how Abaqus proved to be instrumental in successfully meeting these challenges in the context of a representative sunshield film model.

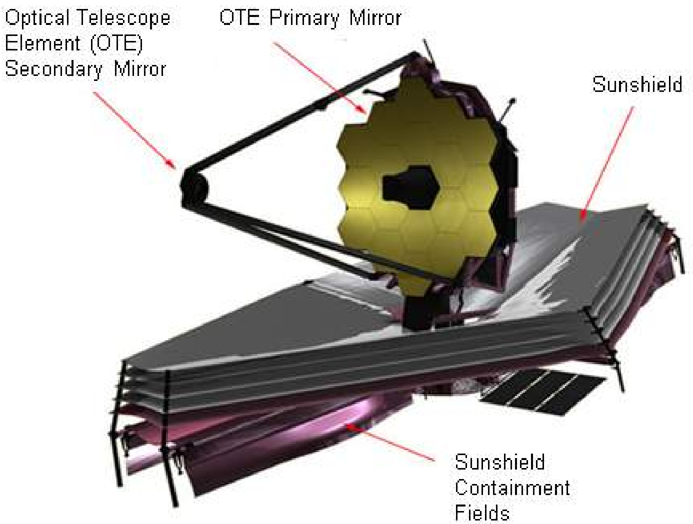

Figure 1. The James Webb Space Telescope.
(http://www.jwst.nasa.gov/observatory.html)

2. Challenges for Sunshield Fold & Deployment Simulation

Accurately simulating the folding and deployment response of the sunshield poses the following challenges:

1. Although the bending stiffness of film is small relative to its membrane stiffness, it does play key role in the both the formation of edge folds during stowage and unfolding/deployment resistance. Therefore, a shell element formulation is necessary versus a simpler, less costly membrane element formulation
2. While the bending stiffness is essential to the physics of the problem, its inclusion poses numerical difficulties since the in-plane (membrane) stiffness is six orders of magnitude higher than bending stiffness it tends to generate an ill-conditioned stiffness matrix. In such cases, efficient convergence of implicit time integration finite element solvers will become increasingly difficult to achieve.
3. The deployment simulation will involve intensive contact calculations with very large amounts of sliding with significant friction. The typical difficulties of such problems are exacerbated here due to the numerical ill-conditioning noted

4. Further, the contact solution should account for shell thickness when shell element formulations are used. Contact tracking problems can arise when multi-layer contact of very thin structures occurs regardless of large sliding complexities. Here, we have both.
5. In view of the above noted challenges, one might be inclined to consider the use of an explicit time integration finite element code (e.g., Abaqus/Explicit. The principal problem with such a choice in this problem is the long time scale of the deployment event compared to the allowable stable time increment size required for explicit solution. Even for a coarse mesh, the stable time increment for this system would be around $2x10^{-5}$ sec. Deployment duration is on the order of 2.5-3 hours requiring $\sim 5x10^{8}$ increments. This leads to inordinately long run times.
6. Depending on the level of mesh refinement desired, the large area (40 feet x 72 feet) and five-layer structure of the sunshield can lead to a model with large number of solution degrees of freedom (DOF). In view of the noted convergence difficulties if an implicit code is used, run times will tend to be more sensitive than usual to increased mesh refinement.

For the purposes of the developing a successful modeling approach to address the above challenges, initial model development focused on a simplified, down-scaled sunshield representation.

3.1 Initial Model: Development

The initial Abaqus finite element model targeted for developing the general approach to solution of the sunshield stowage and deployment was a perfectly flat 1-inch wide, single-layer Kapton strip just over 82.5 inches long held vertically relative to a 120-inch by 400-inch, flat rigid surface with one end just touching the rigid surface (see Figure 2).

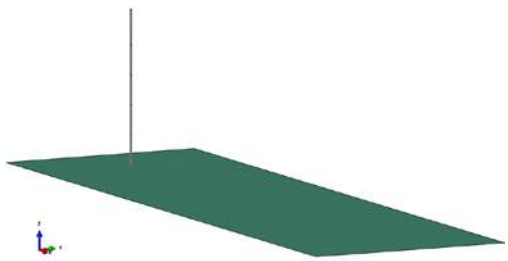

Figure 2. Initial model geometry; Kapton strip in gray and rigid surface in green.

The strip mesh (Figure 3) consists of 374 S4 shell elements (2 across the width, 185 along the length with 4 in the triangular region (Figure 3b) at the free end). As model approaches developed including the choice of contact algorithm the rigid surface might be changed from an analytical rigid body to a discrete rigid body. In cases where a discrete rigid body was warranted, the rigid surface was meshed with 330 R3D4 elements (10 along the 120-inch sides; 33 along the 400-inch sides).

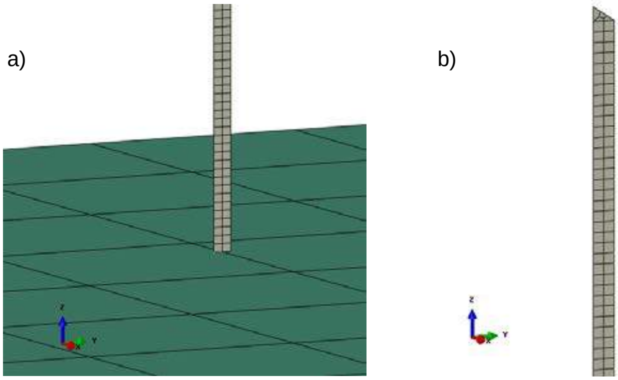

Figure 3. Mesh details: a) Strip end at rigid surface interface, b) Triangular region at the free end of strip.

The shell elements comprising the strip were assigned a shell section property referencing the desired thickness (0.001 inches) and a Kapton material definition including an elastic modulus of 0.9x106 psi, Poisson ratio of 0.32 and mass density of $1.375\text{x}10^{-4}$ $lb_{f.}\text{-}s.^{2}/in.^{4}$.

The analysis encompasses a series of four events:

1. Pre-fold displacement: X-displacements applied as shown in Figure 4 at the noted locations (16-inches apart). This begins the process of simulating the folded or stowed configuration for the simplified strip case.

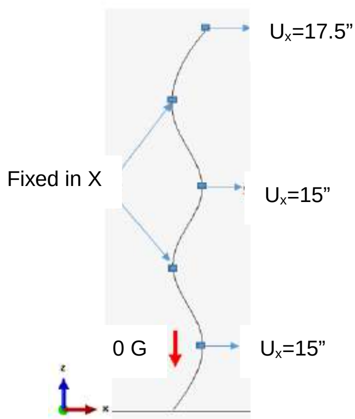

Figure 4. Prescribed conditions pre-fold event.

2. Collapse into a folded configuration from the pre-fold configuration under a 1-G (386.4 in./s^2) gravitational acceleration (in the negative Z-direction) with the intermediate pre-fold displacement locations released to freely deform (Figure 5).

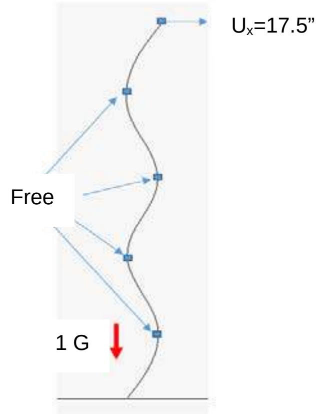

Figure 5. Prescribed conditions for collapse/fold event.

3. Lift the free end of the collapsed/folded strip to a pre-deployment height (about 2.5 inches) maintaining the 1-G loading (simulating Earth-based test environment).
4. Pull the free end out about 80 inches in the X direction to deploy the strip, again while maintaining the 1-G loading over a 9,000 second period.

Each of the above events were captured in separate Abaqus analysis steps. Ultimately, after attempting a variety of analysis procedures for each step, the most successful approach employed Abaqus/Standard for the entire analysis with the first event using the general nonlinear static procedure (**`*STATIC`**) while the remaining three steps used the quasi-static implicit dynamic procedure (**`*DYNAMIC, APPLICATION=QUASI-STATIC`**).

For modeling contact, general contact emerged as preferable to a contact pair formulation in view of its reduced limitations on surfaces, preferable default configuration (surface-to-surface discretization and penalty enforcement) and formulation augmentations allowing for things like edge-to-surface and general ease of set-up. The non-default general contact settings included:

- Feature edge criteria for the strip surface set to 0º (vs. 45º default) to ensure the strip surface is treated as a single contiguous surface without hard fold edges at element edges along the strip length;
- Penalty friction coefficient of 0.3;
- The following additions to the abaqus_v6.env file:

```
import os
os.environ["ABA_GCONT_POOL_SIZE"] = '5'
mp_environment_export = mp_environment_export + ('ABA_GCONT_POOL_SIZE ',)
```

This last item is sometimes required in the current version of Abaqus with general contact when large numbers of contact constraints evolve and is not required for most problems.

The goals of this initial model were 1) to achieve a successfully converged result for all four steps of the event sequence, 2) for that result to adequately represent the actual physics of the membrane deployment and 3) develop insights on modeling techniques useful in scaling up the model.

3.2 Initial Model: Results

The initial model was run successfully using Abaqus 2016 (Beta 3) on a Linux computer employing 2 cores for solution. Total wall-clock time for solution was19 hours and 43 minutes.

Figure 6 shows the evolution of the deformed shape of the strip over steps 1 through 3. Figure 7 shows selected snapshots of the progressing deformation along with the deployment “pull” force history during step 4. Note the oscillatory “noise” the solution generates. This is apparently due to combined stick/slip, structural oscillation (exacerbating stick/slip) and discretization effects (e.g., mesh refinement).

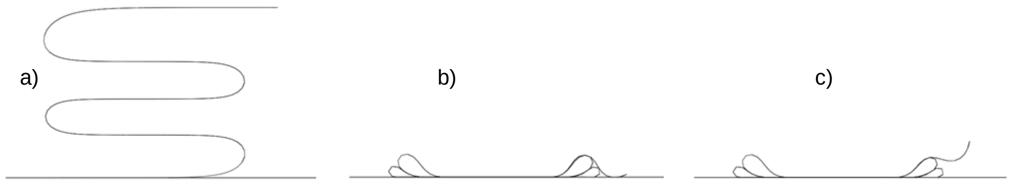

Figure 6. Deformed shape at a) end of Step 1, b) end of Step 2 and c) end of Step 3.

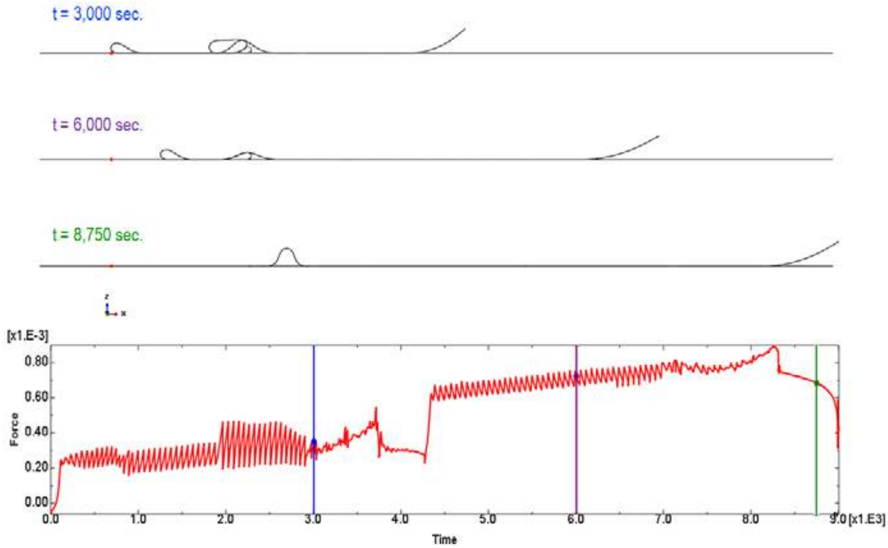

Figure 7. Deformation and pull force history for Step 4.

Refining the mesh was shown to minimize the magnitude of the oscillations but the underlying trend of the response was the same in both the original mesh configuration and the finer variant (2X the coarse mesh element count in both length and width directions) as illustrated in Figure 8. It should be noted that the finer mesh variant increased run-time to about 56 hours (wall-time) using 16 cores.

Figure 8. Pull force vs. displacement for original coarse mesh vs. refined mesh.

Figure 9 shows the kinetic, strain and friction dissipation energy histories. Kinetic energy content is negligible and the problem is dominated by frictional dissipation. Strain energy history is characterized by a series of staged energy release events associated with the pulling out of the individual folds in the strip over step 4.

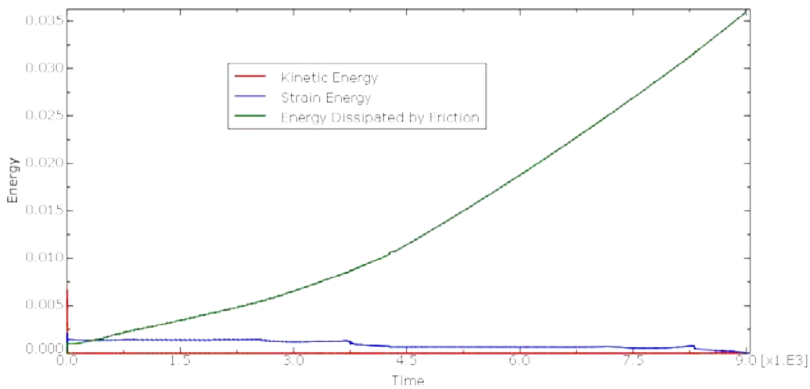

Figure 9. Energy histories.

4. Model Scale-up

A series of models were developed after the initial model to both explore efficient modeling techniques and add more complete details of the full sunshield. To reduce computation cost, a wide 5-layer membrane construction was approximated via an equivalent single layer one inch wide strip finite element representation. A connector-based technique was implemented to model the spiral spring mechanisms which are attached to the sunshield to control billowing during deployment in the 0-g environment of space. These models culminate in the so-called Zone 1 Simulator model.

4.1 Model Reduction with Equivalent Thickness/Width Approach

As more elaborate models were constructed including the five Kapton layers of the sunshield and larger plan-forms, the proliferation of both degrees of freedom and contact calculations rapidly drives model run-times beyond acceptable bounds for use within the JWST program. It was evident some form of simplification would need to be introduced to facilitate scaling the problem up.

The principal simplification used was to use a single-layer narrow strip with width W_{eq} and equivalent properties to mimic the in-plane stiffness, bending stiffness and total weight of a five-layer wide section with width W. Additionally, a bending stiffness correction factor, C_f, was applied to account for partial shear-tie between sunshield layers due to friction. It was determined from the ratio of the radii of the fold between a five-layer strip model and single-layer strip model subjected to 1G. For a friction coefficient of 0.3, C_f is determined to be 1.24.The equivalent properties are derived from the following equivalency relations for in-plane stiffness, bending stiffness and mass:

$$E_{eq} \cdot t_{eq} \cdot W_{eq} = E \cdot (n \cdot t_1 + t_2) \cdot W \qquad (1)$$

$$E_{eq} \cdot {t_{eq}}^3 \cdot W_{eq} = C_f \cdot E \cdot (n \cdot {t_1}^3 + {t_2}^3) \cdot W \qquad (2)$$

$$\rho_{eq} \cdot t_{eq} \cdot W_{eq} = \rho \cdot (n \cdot t_1 + t_2) \cdot W \qquad (3)$$

Where E is the elastic modulus, t is thickness, ρ is mass density of the Kapton layers, n is the number of thinner, cold-side sunshield layers and W is width. The thicknesses t_1 and t_2 are the thicknesses of the cold-side sunshield layers (each 0.001 inch) and the sun-facing layer (0.002 inch thick), respectively. The "*eq*" subscripted quantities are the equivalent properties to be calculated and used in the equivalent finite element model.

The above lead to the following expressions for the equivalent properties:

$$E_{eq} = \left(\frac{W}{W_{eq}}\right) \cdot E \cdot (n \cdot t_1 + t_2) \cdot \sqrt{\frac{(n \cdot t_1 + t_2)}{C_f \cdot (n \cdot {t_1}^3 + {t_2}^3)}} \qquad (4)$$

$$t_{eq} = \sqrt{\frac{C_f \cdot (n \cdot {t_1}^3 + {t_2}^3)}{(n \cdot t_1 + t_2)}} \qquad (5)$$

$$\rho_{eq} = \left(\frac{W}{W_{eq}}\right) \cdot \frac{\rho \cdot (n \cdot t_1 + t_2)}{t_{eq}} \qquad (6)$$

E_{eq} and ρ_{eq} will be used to define a new, equivalent material property for use in the Abaqus model while t_{eq} will be used to define the shell section thickness for the single-layer strip shell elements. The final modification to be included in the equivalent property finite element model is to adjust the thickness used in the contact calculations to reflect the true sunshield thickness (i.e., $n \cdot t_1 + t_2$) not t_{eq}. This is done via the `*SURFACE PROPERTY ASSIGNMENT, PROPERTY=THICKNESS` keyword.

4.2 Function and Idealization of Spiral Spring Mechanism

The strain energy stored in the stowed/folded sunshield film layers during the packaging of the assembly in the 1-g environment of Earth must be managed by a series of mechanisms during deployment in the 0-g environment of space in order to prevent billowing and allow a controlled deployment sequence. Each of these is similar to a torsionally sprung fishing reel with the reel drum fixed to the sunshield deck and the end of the "fishing line" attached to a point on the sunshield film. Further, the end of the line breaks away from the sunshield when the axial load in it exceeds a certain critical level.

Two approaches to modeling these spiral spring mechanisms were developed, one more computationally expensive but of higher fidelity and the other less expensive but with additional simplifying approximations. Both rely on the use of Abaqus connector elements.

The more complex approach, referred to as the "coil-spring method", is illustrated in Figure 10. The key elements of this approach include1) a discretized rigid 2-inch diameter cylindrical mandrel on which 2) a series of connected beam elements (representing a 0.005 inch x 1.5 inch Kapton ribbon) is helically wound with 3) a **`HINGE`** connector with nonlinear stiffness and damping behavior to control rotation of the mandrel and 4) an **`AXIAL`** connector at the free end of the beam elements with a 1.5-lb$_f$. failure behavior to facilitate break-away response. The beam and discrete rigid elements are included in the general contact domain so that interaction between the reeled ribbon, the Kapton sunshield film and the mandrel are captured (but beam-to-beam interaction is neglected).

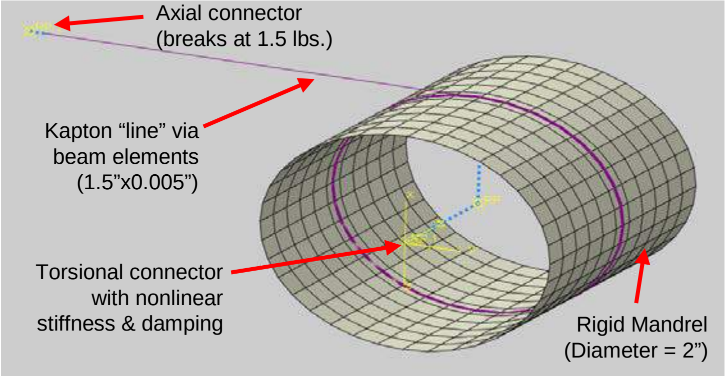

Figure 10. The "coil-spring method" for spiral spring mechanism modeling.

The simpler approach, referred to as the "axial spring method", just uses a single **`AXIAL`** connector including appropriate nonlinear stiffness and failure behaviors for each mechanism occurrence with one end node fixed to the sunshield deck and the other to the attachment point on the sunshield film.

In both methods, the **`*MODEL CHANGE`** keyword is used to control activation of the **`AXIAL`** connector element after the 1-g folded/stowed configuration has been resolved but prior to the removal of the 1-g load and initiation of the deployment sequence.

4.3 Zone 1 Simulator Model: Development

This phase of the analysis effort culminated in the Zone 1 Simulator model using Abaqus/Standard (2016 GA release) and illustrated in Figures 11 and 12. It consists of a discrete rigid deck and IVA (Integrated Verification Article) table (totaling 162 R3D4 elements), the sunshield film approximation (848 S4R elements) and a series of spiral spring mechanisms modeled using the "axial spring method" (13 connector elements; 6 outboard, 7 inboard). The sunshield film approximation represents the 5-layer, 80-inch wide construction via a combination of a **ZSYMM** boundary condition and the previously described equivalent property method with the following equivalent properties:

$$E_{eq} = 137.2 \text{ Msi}; \quad t_{eq} = 0.001575\text{in.}; W_{eq} = 1\text{in.}; \rho_{eq} = 0.0209 \text{ lb}_f \text{-s}^2/\text{in.}^4.$$

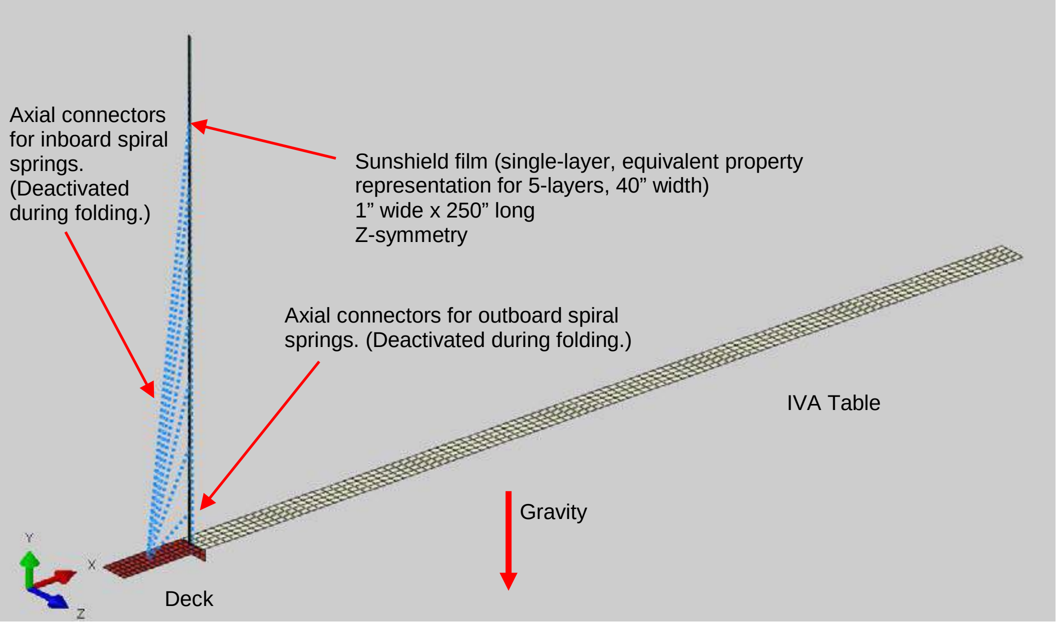

Figure 11. Zone 1 Simulator model.

All contact interactions are handled by the general contact algorithm with a universal penalty friction coefficient of 0.3 and using the default penalty stiffness for normal-direction contact enforcement. Additionally, the feature edge criterion for the sunshield surface is modified from the default value of 45° to be 0° and the sunshield surface property assignment corrects the contact thickness to the true film thickness (i.e.,$t_{5\text{-layer}}$= 0.006 in.) by using the scaling factor of 3.81 (i.e., $t_{5\text{-layer}}/t_{eq}$ = 0.006 inch/0.001575 inch). Finally, to allow for the very large number of evolving contact constraints unique to this problem the ABA_GCONT_POOL_SIZE environment parameter was set to 100.

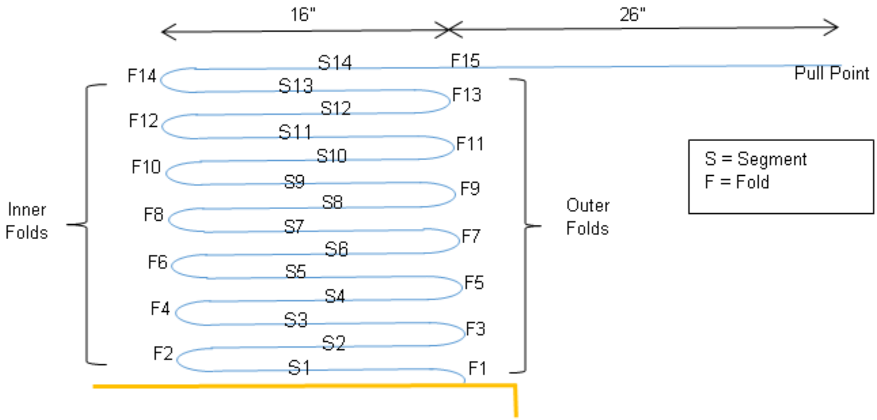

Figure 12. Schematic of 14-fold pre-fold configuration for Zone 1 Simulator model.

As described in prior sections, the analysis event history is segmented into an appropriate series of analysis steps covering approximately 12,000 seconds of event time (most of which is in deployment). For the Zone 1 Simulator model, each step used the quasi-static implicit dynamic procedure. Finally, as noted in the previous section, **`*MODEL CHANGE`** is used in the appropriate analysis steps to control deactivation and activation of the **`AXIAL`** connectors coupling the spiral spring mechanisms to the sunshield film.

4.4 Zone 1 Simulator Model: Results

Results were generated with the Zone1 Simulator model for two principal cases: 1) deployment in a 1-g environment (Earth test) and 2) 0-g on-orbit deployment. Figure 13 characterize the deformed state of the sunshield film in the stowed configuration.

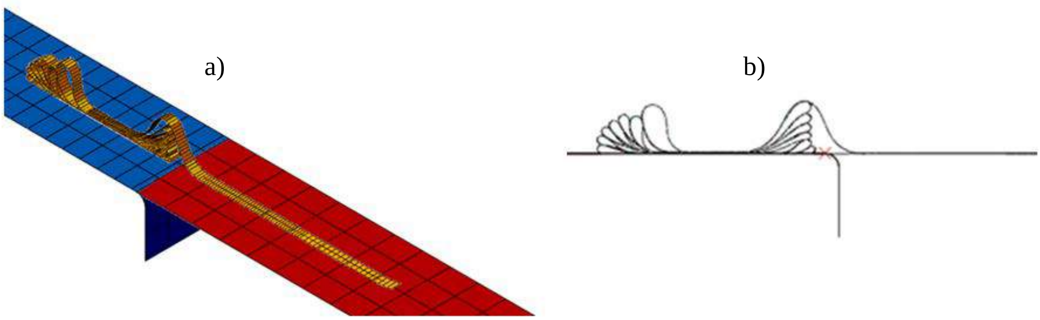

Figure 13. Deformed state of Zone 1 Simulator sunshield film in stowed configuration, a) isometric and b) side views.

Figures 14-16 show characteristic deformation evolution and deployment force history results at selected time points for the 1-g "Earth test" environment case.

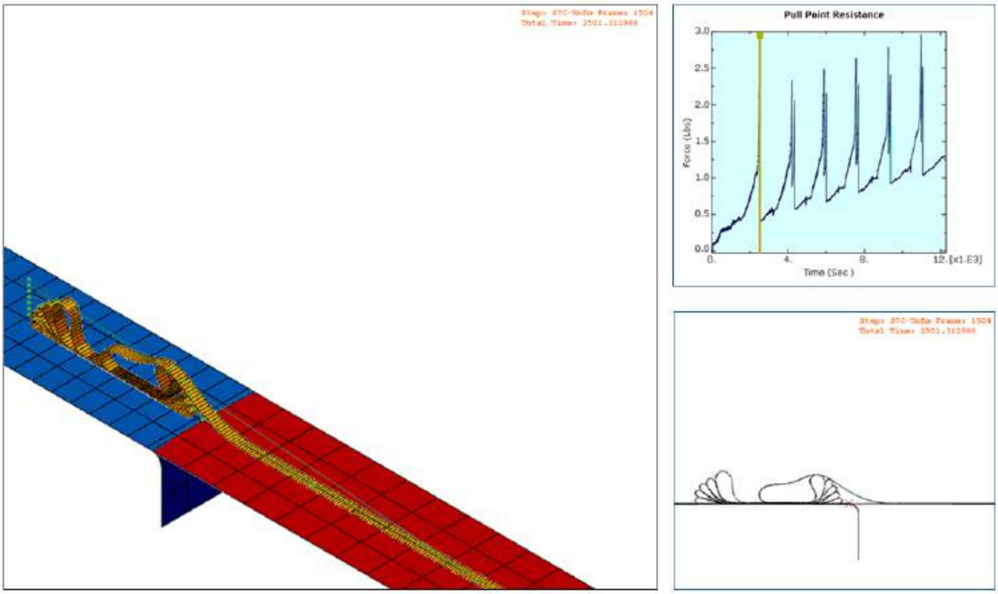

Figure 14. Zone1 Simulator results at t=2,501 sec.

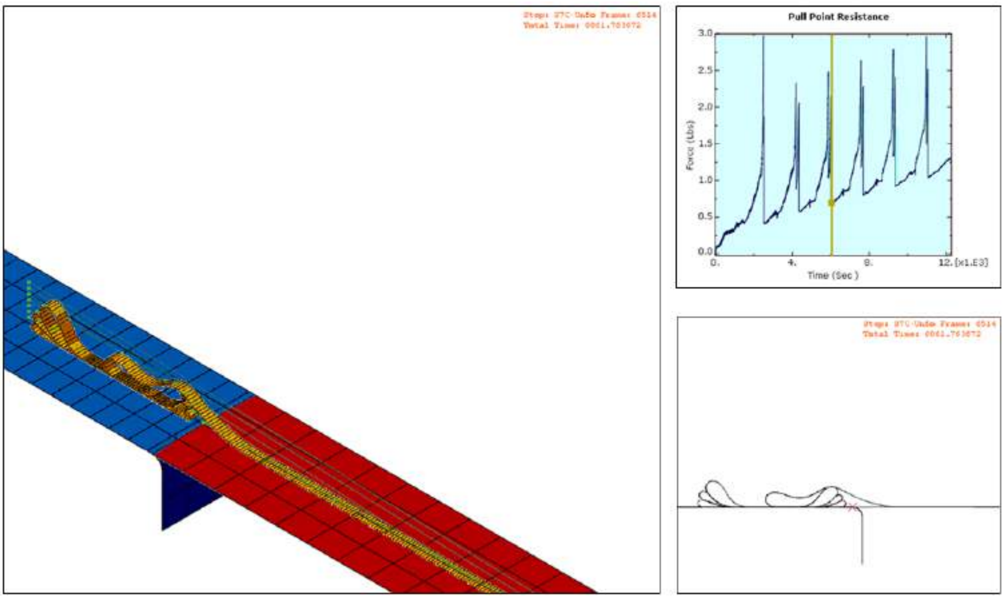

Figure 15. Zone1 Simulator results at t=6,062 sec.

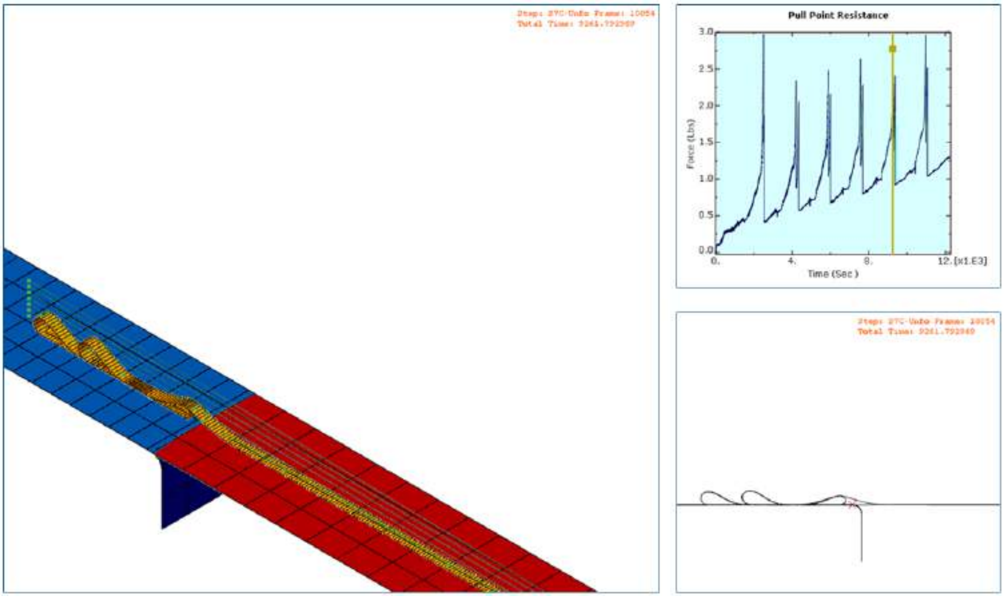

Figure 16. Zone1 Simulator results at t=9,262 sec.

In addition to ensuring generally smooth deployment of the sunshield, characterization of the deployment pull force is of principal interest in order to ensure proper sizing of surrounding structure and actuating mechanisms. As such, validation of the Abaqus-generated results against accepted closed-form deployment resistance calculations were performed. These calculations account for gravity, friction and multiple folds and include resistance of spiral springs and clip release. The deployment force, R is a linear combination of the frictional resistance of the film over the slipping area (R_f)and the sum of the spiral spring forces (R_s)in the deployment direction, both of which are functions of the current deployment displacement, x.

The relations in detail are:

$$R(x) = R_f(x) + R_s(x) \quad (7)$$

$$R_f(x) = \mu t W \rho g \, (L_0 + x) \quad (8)$$

$$R_s(x) = \sum_{i=1}^{n} R_{s\,i}(x) \quad (9)$$

where μ is friction coefficient, t is film thickness, W is film width, ρ is film mass density, g is the gravitational acceleration, L_0 is the initial film length in contact and R_{si} is the spring resistance of the i-th spiral spring. Obviously, in the 0-g environment these relations indicate the frictional resistance to be zero.

Figures 17 and 18 compare the closed form and Abaqus predicted deployment forces for both the 1-g and 0-g environment cases. Figure 17 includes the closed form result for only the friction contribution to more readily illustrate the effect of its absence in the 0-g case. The inset image in Figure 17 shows the state associated with the “notch” in the Abaqus-predicted response which suggests that the release of strain energy in the film at that particular configuration along with the tension of the outboard springs likely allowing film displacement for a short time with no additional added deployment force until the system moves into a new configuration at which point begins to force build again. Other than this “notch” behavior, the comparisons indicate very good agreement between the closed form and Abaqus predictions, bolstering confidence in the validity of the Abaqus model and the approaches used therein.

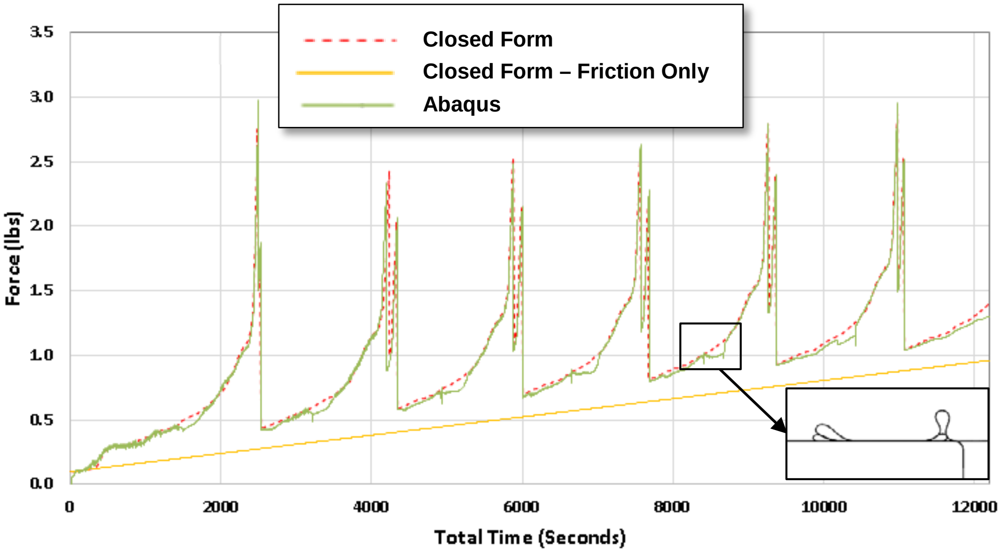

Figure 17. Deployment force comparisons for 1-g case.

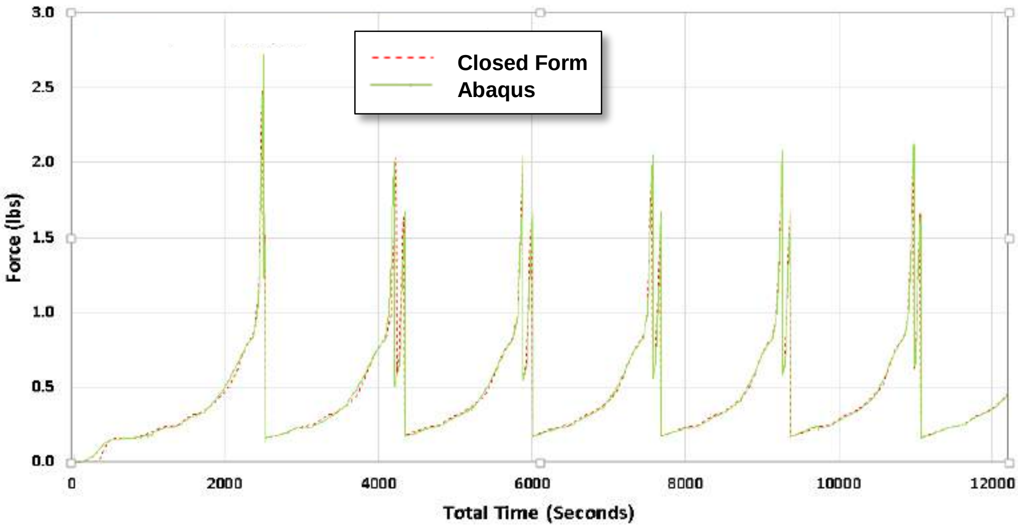

Figure 18. Deployment force comparisons for 0-g case.

5. Conclusions

A modeling approach using Abaqus/Standard was developed and successfully demonstrated as being a useful tool in the simulation of the folding/unfolding behavior of the JWST sunshield membrane which has smooth folds and uniform cross section. The demonstration included validation by comparing the deployment force from the model against a closed form solution.

While the size of the model in terms of user-defined degrees of freedom gives the false impression of relative simplicity, the problem addressed is extremely challenging for commercial finite element analysis products particularly due to the combined complexity of the contact behavior and the ill-conditioning of the finite element stiffness matrix required to capture the structure's membrane-bending response. The success of the current work is a testament to both the power and robustness of Abaqus/Standard solution technology and the expertise of well-trained users.

In spite of the noted power of the software, the computational cost of the analyses considerable reliance on user expertise and innovation for the development of reasonable cost-saving simplifications to the model. In future, it is hoped that further advances in Abaqus solution technology and further user experimentation with parallel solution and alternate modeling approaches will reduce model run times. Desired advances in Abaqus technology include automatic re-sizing of the general contact constraint pool as a contact solution evolves.

Acknowledgements

The authors would like to thank Harry Harkness and George Ang of the SIMULIA R&D team without whose help some of the contact hurdles posed by this uniquely challenging problem could not have been successfully addressed.